AGU100 ADVANCING EARTH AND SPACE SCIENCE

Geophysical Research Letters

RESEARCH LETTER
10.1029/2018GL080258

Key Points:
- Modeling of cerean faulted topography suggests that its surface is elastically similar to many of the icy satellites of Jupiter and Saturn
- The near surface of Ceres at Nar Sulcus is likely ice-rich and contains less than ~30 vol.% mechanically silicate-like phases
- We estimate the surface heat flux at Nar Sulcus during its formation to be ≥10 mW/m^2

Supporting Information:
- Supporting Information S1
- Data Set S1
- Data Set S2
- Data Set S3
- Data Set S4
- Data Set S5
- Data Set S6
- Data Set S7
- Data Set S8
- Data Set S9
- Data Set S10
- Data Set S11
- Data Set S12
- Data Set S13
- Data Set S14
- Data Set S15
- Data Set S16
- Data Set S17
- Data Set S18
- Data Set S19
- Data Set S20
- Data Set S21
- Data Set S22
- Data Set S23
- Data Set S24

(continued)

Correspondence to:
K. H. G. Hughson,
p151c@ucla.edu

Citation:
Hughson, K. H. G., Russell, C. T., Schmidt, B. E., Travis, B., Preusker, F., Neesemann, A., et al. (2019). Normal faults on Ceres: Insights into the mechanical properties and thermal history of Nar Sulcus. *Geophysical Research Letters*, 46, 80–88. https://doi.org/10.1029/2018GL080258

Received 29 AUG 2018
Accepted 20 NOV 2018
Accepted article online 26 NOV 2018
Published online 6 JAN 2019

Normal Faults on Ceres: Insights Into the Mechanical Properties and Thermal History of Nar Sulcus

Kynan H. G. Hughson[1], C. T. Russell[1], B. E. Schmidt[2], B. Travis[3], F. Preusker[4], A. Neesemann[5], H. G. Sizemore[3], P. M. Schenk[6], D. L. Buczkowski[7], J. C. Castillo-Rogez[8], and C. A. Raymond[8]

[1]Department of Earth, Planetary, and Space Sciences, University of California, Los Angeles, CA, USA, [2]School of Earth and Atmospheric Sciences, Georgia Institute of Technology, Atlanta, GA, USA, [3]Planetary Science Institute, Tucson, AZ, USA, [4]German Aerospace Center (DLR), Berlin, Germany, [5]Institute of Geological Sciences, Planetary Sciences and Remote Sensing, Freie Universität Berlin, Berlin, Germany, [6]Lunar and Planetary Institute, Houston, TX, USA, [7]Johns Hopkins Applied Physics Laboratory, Laurel, MD, USA, [8]Jet Propulsion Laboratory, Pasadena, CA, USA

Abstract We characterized two sets of extensional faults that comprise the Nar Sulcus region of Ceres by applying a cantilever model for fault related flexure and derived flexural rigidity values for Nar Sulcus between $2.0 \cdot 10^{15}$ and $1.8 \cdot 10^{16}$ N·m. This range of flexural rigidity makes Nar Sulcus mechanically akin to extensional structures on Ganymede, Europa, and Enceladus. We combine these observations with an inferred strength profile for the upper mechanical layer of Ceres and estimate its thickness to be 2.9–9.5 km. Surface heat fluxes at Nar Sulcus during its formation were likely ≥10 mW/m^2 for estimated strain rates of 10^{-17}–10^{-14} s^{-1}, which is at least one order of magnitude larger than the current estimated global average. For geologically plausible heat fluxes between 10 and 100 mW/m^2, we estimate an upper bound of ~30 vol.% mechanically silicate-like phases in the near surface at Nar Sulcus, neglecting the effects of porosity.

Plain Language Summary In March 2015, the National Aeronautics and Space Administration's Dawn spacecraft began orbiting the dwarf planet Ceres, the largest object in the main asteroid belt between Mars and Jupiter. Research has shown that a major volume fraction of the subsurface of Ceres may be composed of water ice. Knowing how water ice is distributed in the upper layer of Ceres is essential to understanding how the surface and interior have evolved over time. The Nar Sulcus region consists of two sets of extensional faults that we characterized in this study. We modeled the topography of these extensional faults in order to determine the elastic properties of the region. The properties we derived for Ceres' uppermost mechanical layer are similar to those of many of the icy moons of Jupiter and Saturn. Furthermore, they were used to help constrain three key parameters of this upper layer at Nar Sulcus: its mechanical thickness, its heat flow during the formation of the faults, and its water ice volume fraction.

1. Introduction

Upon arriving at the dwarf planet Ceres in March of 2015, the National Aeronautics and Space Administration's Dawn mission (Russell et al., 2016) discovered an intensely fractured region in Ceres' southern hemisphere now named Nar Sulcus (Crown et al., 2017). The Nar Sulcus fractures (Figure 1), which are centrally located at 280.11°E, 41.86°S within the Yalode impact crater, display morphologies similar to those of imbricated listric normal faults on the Earth and have topographic profiles suggestive of elastic flexure. Modeling the shape of elastically flexed topography allows for the estimation of the elastic thickness of the mechanical layer being faulted. When this elastic thickness is combined with an assumed strength profile and strain rate, the mechanical thickness and heat flux present at the site of the newly formed topography can be estimated. Estimates of these parameters through the analysis of flexurally supported topography have previously been done on the Earth (e.g., Kusznir et al., 1991; Lowry & Smith, 1994; Weissel & Karner, 1989), Venus, (e.g., O'Rourke & Smrekar, 2018), Mars (e.g., Grott et al., 2005; Ruiz et al., 2006), Ganymede (Nimmo & Pappalardo, 2004; Nimmo et al., 2002), Europa (Nimmo & Schenk, 2006; Ruiz, 2005), Tethys (Giese et al., 2007), and Enceladus (Giese et al., 2008). Despite a plethora of evidence suggesting Ceres' upper layer is rich in water ice (e.g., Buczkowski et al., 2016; Combe et al., 2016, 2019; Fu et al., 2017; Hughson et al., 2018; Prettyman et al., 2017; Schmidt et al., 2017; Sizemore et al., 2017, 2018), its exact concentration and

10.1029/2018GL080258

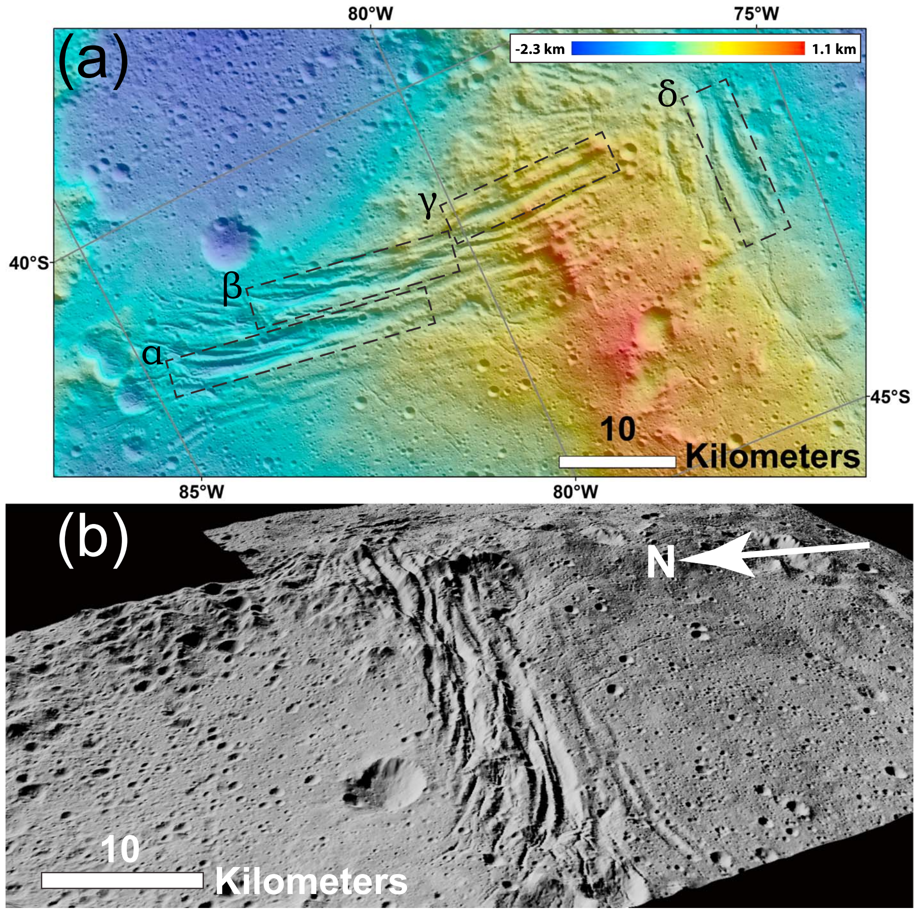

Figure 1. (a) Plan view of the Nar Sulcus fractures (from the Ceres low altitude mapping orbit clear filter mosaic, resolution ~35 m per pixel; Roatsch et al., 2016b) overlain by color-coded stereo-topography relative to the 482 km by 446 km oblate best-fit biaxial ellipsoid (vertical accuracy <10 m). The dashed boxes indicate the largest faults examined in this study. These valleys were unofficially named α, β, γ, and δ valles. Stacked topographic profiles for each valley were created from transects spaced 1 km apart oriented perpendicular to the long axis of each rectangle (see Supporting Information S1 for more information). (b) Perspective view of the largest faulted set at Nar Sulcus from the west looking east. The vertical exaggeration in this view is a factor of 1.5.

distribution remains enigmatic. Flexural analysis of Nar Sulcus presents a unique opportunity to better understand the role of water ice on the surface geology of Ceres, at least locally to this unique landform.

We present new elastic constraints on the upper mechanical layer of Ceres proximal to Nar Sulcus. We use stereophotogrammetrically derived elevation models (Roatsch et al., 2016a) to identify two sets of possible normal faults on Ceres, analyze them for topography that is flexurally supported, and use that topography to obtain estimates of the effective elastic thickness and surface heat flux range proximal to Nar Sulcus at the time of their formation. In order to better constrain the role of ice in the upper layer of Ceres, this exercise is repeated at strengths and rheologies approximating ice-rock mixtures with 0, 30, and 56 volume percent rock. Additionally, we estimate the time at which these parameter estimates are valid by applying a Buffered Crater Counting (BCC) approach (Fassett & Head, 2008; Kneissl et al., 2015), specifically designed to derive crater-based absolute model ages of narrow linear features.

2. Observations

Nar Sulcus was extensively imaged by Dawn's framing cameras throughout its mission at resolutions as fine as ~35 m per pixel. This region consists of two mutually perpendicular sets of fractures located just north of a large (~2 km tall) tholus. The larger of these sets trends approximately east-west, is ~50 km long, and ~10 km

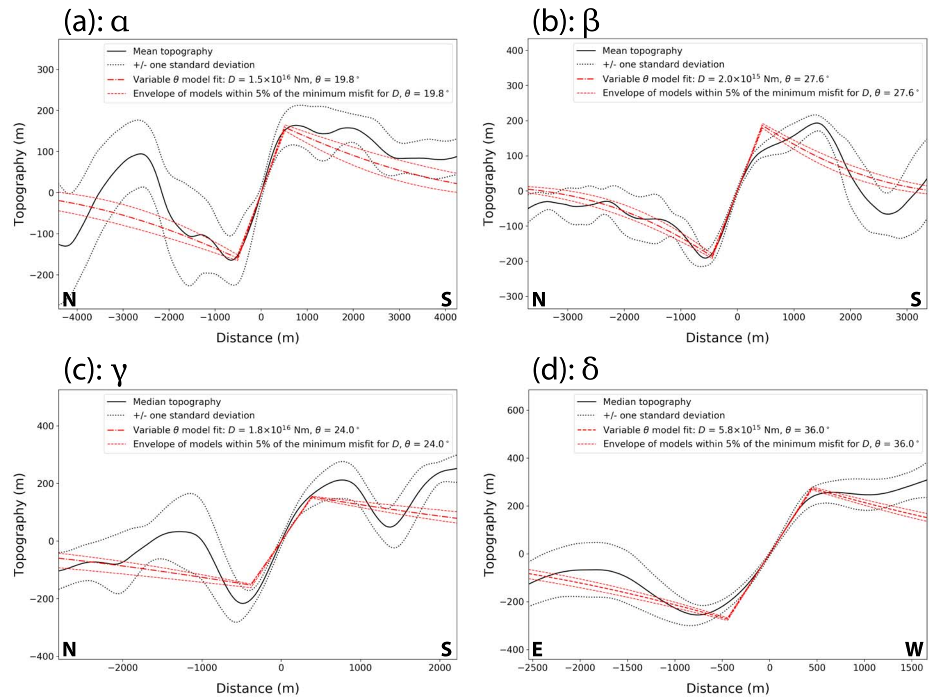

Figure 2. Stacked topographic profiles across the four valleys identified in Figure 1a. Black-solid lines depict mean topographies, black-dotted lines are ±one standard deviation from the mean topographies, reported θ values are the minimum root-mean-square misfit dip angles for the faults, and the red dash-dotted lines depict best fit (minimum root-mean-square misfit) profiles from the flexural cantilever model. All model solutions at the given θs whose misfits are within 5% of the minimum misfit cases exist between the red-dashed lines in each subfigure (see Figure S3 for further details on misfit uncertainties). Bold letters represent the approximate cardinal direction along each profile. (a) depicts α valles, $D = 1.5^{+3.0}_{-1.0} \cdot 10^{16}$ N·m; (b) depicts β valles, $D = 2.0^{+1.5}_{-0.9} \cdot 10^{15}$ N·m; (c) depicts γ valles, $D = 1.8^{+8.0}_{-1.0} \cdot 10^{16}$ N·m; and (d) depicts δ valles, $D = 5.8^{+4.0}_{-2.0} \cdot 10^{15}$ N·m.

wide. The smaller set trends approximately south-north, is ~15 km long, and ~10 km wide. Stereo-topography (Roatsch et al., 2016a) revealed the major fractures in both sets to have characteristic vertical displacements (throws) between 400 and 550 m, horizontal displacements (heaves) between 800 and 1,000 m, and spacings of ~1.5–2 km. The morphology of these well-defined sets of subparallel ridges and troughs is consistent with an origin due to extensional faulting. The consistent concave down shape of the downthrown fault blocks and concave up shape of the upthrown fault blocks further suggest flexurally supported topography (Giese et al., 2007, 2008).

Previous studies reported a model age of 580 Ma for Yalode ejecta and 420 Ma for the Urvara/Yalode smooth material unit which hosts Nar Sulcus, using a lunar-like impact chronology (Crown et al., 2017). However, this smooth material may have a model age as young as 190 Ma (Crown et al., 2017). We performed a Buffered Crater Counting analysis of Nar Sulcus and its surrounding terrain for craters with diameters ≥200 m using both a Lunar Derived and Asteroid Derived chronology model (Hiesinger et al., 2016) in order to establish their chronostratigraphic relationship (supporting information Figure S1). The derived model age ranges for Nar Sulcus and the background material are 98–173 and 165–478 Ma, respectively. From this analysis, we conclude that Nar Sulcus is temporally distinct from its immediate surroundings and is considerably younger than Yalode.

3. Methods

We estimate the elastic thickness, T_e, of the upper mechanical layer proximal to Nar Sulcus by applying a single layer flexural cantilever model similar to the one developed by Kusznir et al. (1991) to stacked topographic profiles of the four largest fault-bound valleys in Nar Sulcus (Figure 2, see Figure 1a for context). The details of this model are described in Text S1. We infer T_e at Nar Sulcus from model derived values of the flexural rigidity (D) and surface fault dip angle (θ) and from imposed values of the material's Young's modulus (E) and Poisson's ratio (υ). The relationship between these material properties is given by (1).

$$D = \frac{E \cdot T_e^3}{12 \cdot (1 - \nu^2)}. \tag{1}$$

In order to estimate the heat flux and mechanical thickness, T_m, of the surface near Nar Sulcus, we implement McNutt's (1984) model of the vertical structure of the lithosphere. In this formalism strain is accommodated through brittle sliding in an upper fractured layer, through flexure of an underlying elastic layer, and finally by ductile flow within the bottommost region. The mechanical thickness is defined as the high strength region of Ceres from its surface down to where ductily supported stresses at geologically relevant strain rates are negligible. On Earth, this is taken to be ~50 MPa (McNutt, 1984). We choose this limiting stress on Ceres to be 1 kPa, which is small compared to the average maximum modeled differential stress of several hundred kilopascals. The dependence of T_m on the limiting stress is weak given that material strength falls off rapidly with increasing temperature. We use the relationship between T_m and T_e established by Giese et al. (2007, 2008) given by (2).

$$T_e = \left\{ \frac{12 \cdot (1 - \nu^2)}{E \cdot K_{\max}} \cdot \int_0^{T_m} [\sigma(z) \cdot (z - z_n)] dz \right\}^{\frac{1}{3}}, \tag{2}$$

where $\sigma(z)$ is the differential stress at a depth z taken to be the least of the aforementioned brittle sliding stress, elastic stress, and ductile stress of the mechanical layer. $K_{\max}$ is the maximum curvature of either the upthrown or downthrown fault block's profile derived from the flexural cantilever model, and z_n is the depth to the neutral axis (i.e., the depth where the stress changes from compressional to extensional in a bent plate with positive curvature) such that the stress profile integrates to 0.

To generate the stress profile $\sigma(z)$, we adopt the brittle strength relations for cold ice given by Beeman et al. (1988) with a slope of 0.69 and an intercept equal to 0. Changing the slope to 0.85, which is representative of most competent silicate materials (Byerlee, 1978), changes the value of T_e for a given heat flux by only ~1%. For the ductile strengths, we consider grain boundary sliding and dislocation creep via the following equation

$$\dot{\varepsilon} = \dot{\varepsilon}_{\text{gbs}} + \dot{\varepsilon}_{\text{disl}}, \tag{3}$$

where $\dot{\varepsilon}$ is the average strain rate during the formation of Nar Sulcus and $\dot{\varepsilon}_{\text{gbs/disl}}$ are the specific strain rates associated with grain boundary sliding (gbs) and dislocation creep (disl). These strain rates can be written generally as the following (Giese et al., 2007, 2008; Goldsby & Kohlstedt, 2001; Ranalli, 1995)

$$\dot{\varepsilon} = A \cdot \left(\frac{\sqrt{3}}{2} \right)^{n+1} \cdot \left(\frac{1}{d} \right)^m \cdot \sigma_{\text{ductile}}(z)^n \cdot e^{\left(\frac{-Q}{R \cdot T(z)} \right)}, \tag{4}$$

where R is the gas constant, $T(z)$ is the temperature at depth z, d is the grain size, and Q is the process dependent activation energy. A, n, and m are all process and material dependent constants. $T(z)$ is related to the heat flux, F, via (5)

$$F = k_m \cdot \frac{\partial T}{\partial z}, \tag{5}$$

where k_m is the thermal conductivity of the mechanical layer. We use McCord and Sotin's (2005) thermal conductivity for an ice-silicate mixture

$$k_m = 4.2 \cdot f_s + (1 - f_s) \cdot \left(0.4685 + \frac{488.12}{T(z)} \right), \tag{6}$$

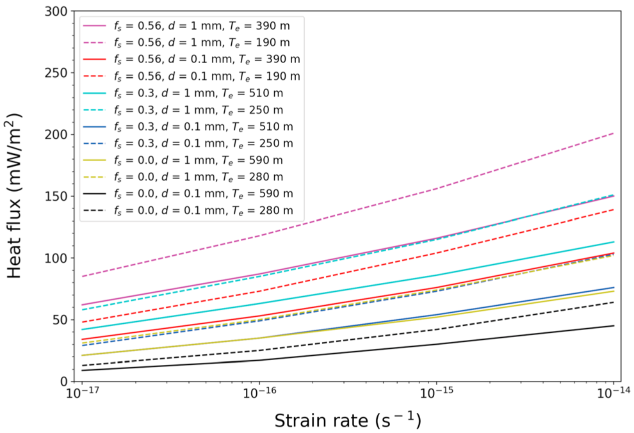

Figure 3. Surface heat flux as a function of strain rate from (2) for different combinations of f_s, T_e, and d. The dashed and solid lines of a given color represent the bounding values of T_e measured at Nar Sulcus for the chosen values of f_s and d; thus, they encapsulate the full range of possible heat fluxes at a given strain rate for those parameter choices.

where f_s is the silicate volume fraction, and k_m is measured in watts per meter per kelvin. Our model does not include the effects of porosity due to its unknown and likely complex structure; however, we discuss its potential influence on our results in section 5.

Throughout all the above calculations, we use the following values: E_{ice} = 1.0 GPa (Giese et al., 2007, 2008; Nimmo & Pappalardo, 2004; Nimmo & Schenk, 2006), g = 0.28 m/s^2 (Russell et al., 2016), ρ_c = 1,287 kg/m^3 (Ermakov et al., 2017), υ = 0.33 (Giese et al., 2008), d = 0.1–1.0 mm, surface temperature T_s = 150 K (Hayne & Aharonson, 2015), n_{gbs} = 1.8, n_{disl} = 4, m_{gbs} = 1.4, m_{disl} = 0, Q_{gbs} = 49 kJ/mol, Q_{disl} = 60 kJ/mol, A_{gbs} = 3.9 · 10^{-3} MPa^{-n}·m^{m}·s^{-1}, and A_{disl} = 4.0 · 10^5 MPa^{-n}·m^{m}·s^{-1} (the latter eight values are from Goldsby & Kohlstedt, 2001).

To test mechanical layer compositions with rock volume fractions of f_s = 0.30 and f_s = 0.56, we increase the Young's modulus of the mechanical layer by a factor of 1.5 and 3.5, respectively, relative to that of pure ice (Durham et al., 1992; Yasui et al., 2017). Additionally, we increase the effective viscosity for f_s = 0.30 and f_s = 0.56 mixtures by factors of 5 and 150, respectively, relative to the rheology of pure ice (Durham et al., 1992). This is accomplished by multiplying the ductile stress component of $\sigma(z)$ by the previous factors when solving equation (2).

4. Results

Figure 2 displays the results of applying the flexural cantilever model to stacked topographic profiles of the four largest valleys in Nar Sulcus (see Figure 1a). The minimum misfit models return D values ranging from $2.0^{+1.5}_{-0.9} \cdot 10^{15}$ (β valles) to $1.8^{+8.0}_{-1.0} \cdot 10^{16}$ N·m (γ valles). The reported uncertainties in the range of D values are representative of model fits whose root-mean-square misfits for a given D are within 5% of the minimum misfit value for that particular valley at the best fit value for θ, which is analogous to the error reporting approach adopted by Nimmo et al. (2002). Model misfit curves for each analyzed valley are shown in Figures S2 and S3. The maximum absolute curvatures of the valleys derived from model profiles range from $7.6 \cdot 10^{-6}$ (γ valles) to $3.1 \cdot 10^{-5}$ m^{-1} (β valles).

Using the above bounding values for the flexural rigidity, (1) predicts elastic thicknesses proximal to Nar Sulcus within the range of 280^{+70}_{-40}–590^{+900}_{-110}, 250^{+60}_{-40}–500^{+800}_{-100}, and 190^{+50}_{-30}–390^{+600}_{-70} m for a pure ice, f_s = 0.30, and f_s = 0.56 mechanical layer, respectively. The quoted uncertainties in the above values for T_e are propagated from the uncertainties in D using (1). The lower bounds on both D and T_e are well constrained, whereas the upper bounds are less certain.

We estimate the strain in both of Nar Sulcus' fracture sets to be between 5% and 8%. Assuming that Nar Sulcus formed over no less than 0.1 Ma and that it formed over a period of time no longer than our maximum model age estimate of 98–173 Ma, we infer the geologically relevant strain rates in this region at 10^{-17}–10^{-14} s^{-1}. Results from applying the above bounding values of T_e/K_{max} and the aforementioned rheological parameters to (2) are shown in Figure 3. The total range of near-surface heat fluxes that satisfy our mechanical and geological constraints is 9–201 mW/m^2, with associated mechanical thicknesses 2.9–9.5 km. As expected, both the mechanical thickness and the heat flux exhibit considerable dependences on grain size and strain rate.

5. Discussion

Direct comparison of the model derived range of flexural rigidities at Nar Sulcus to other solar system objects firmly characterizes it as mechanically similar to most outer solar system icy satellites (Table 1). In contrast, silicate-dominated bodies like the Earth and Mars have typical flexural rigidities at least four orders of magnitude greater than what we measure at Ceres. Given Ceres' intermediate surface thermal environment between that of the inner and outer solar system, the similarity between the flexural rigidity of Nar Sulcus and those of Ganymede, Europa, and Enceladus suggests that the faulted layer on Ceres is

Table 1
Flexural Rigidities of Various Solar System Objects

Object	D (N·m)	Reference
Ceres (Nar Sulcus)	$2.0^{+1.5}_{-0.9} \cdot 10^{15}$–$1.8^{+8.0}_{-1.0} \cdot 10^{16}$	This study
Ganymede	$5.5 \cdot 10^{14}$–$1.6 \cdot 10^{17}$	Nimmo and Pappalardo (2004)
Europa	$3.0 \cdot 10^{14}$–$1.5 \cdot 10^{17}$	Nimmo and Schenk (2006)
Enceladus	$2.5 \cdot 10^{15}$–$3.9 \cdot 10^{16}$	Giese et al. (2008)
Tethys	$1.1 \cdot 10^{19}$–$3.5 \cdot 10^{19}$	Giese et al. (2007)
Mars	$9.7 \cdot 10^{21}$–$1.7 \cdot 10^{22}$	Grott et al. (2005)
Earth	Typically $> 10^{20}$	For example, Lowry and Smith (1994) and Walcott (1970)

likely a mixture of water ice and denser, more rigid phases, but whose mechanics is dominated by the ice component.

The average near-surface heat flux on Ceres over the past ~800 Myr was likely no greater than ~1 mW/m^2 (Travis et al., 2018). This is in contrast to our results at Nar Sulcus, which are one to two orders of magnitude larger. However, it is possible that eutectic brines currently exist at shallow depths of 30–50 km below the surface (Travis et al., 2018). Stein et al. (2017) postulated that subsurface brines could be brought to the surface or near surface of Ceres following large impact events. Laccolith formation from these fluids could plausibly raise the local heat flux by a few tens of milliwatts per square meter. Similarly, it has been suggested that tholi on Ceres, like the one at Nar Sulcus, may have been formed through solid-state diapirism (Bland et al., 2018), which may have produced a small increase in the local surface heat flux. The emplacement of large quantities of excavated and/or impact heated Urvara/Yalode Smooth Material from the Urvara-forming impact (as suggested by Crown et al., 2017) could have plausibly raised the heat flux at Nar Sulcus by several tens of milliwatts per square meter for potentially a few million years (see Biren et al., 2014, and Bowling et al., 2018, for relevant examples). On this geological basis, we cautiously interpret the local heat flux during formation of the faults to have most likely fallen within 10–100 mW/m^2.

From Figure 3, we note that the only curves which completely satisfy our preferred heat flux range over all geologically relevant strain rates belong to the family f_s = 0.0, with the exception of a single f_s = 0.3 curve. Based on our measured 5–8% strain, $\dot{\varepsilon} = 10^{-15}$ s^{-1} corresponds to deformation on the million-year timescale, which is the relevant heat dissipation timescale for large quantities of material disturbed by the Urvara-forming impact (Biren et al., 2014; Bowling et al., 2018). At this strain rate, we note that all but one of the f_s = 0.3 and only one of the f_s = 0.56 curves in Figure 3 fall below F = 100 mW/m^2. A silicate-dominated rheology at Nar Sulcus is deemed highly unlikely as it would require both an extremely thin elastic layer and an implausibly high heat flux. We estimate an upper bound of ~30 vol.% mechanically silicate-like phases within the mechanical layer at Nar Sulcus, which is broadly consistent with Fu et al.'s (2017) and Ermakov et al.'s (2017) estimate of the global rock volume fraction within the upper layer of Ceres. However, the remaining ~70 vol.% of the mechanical layer in our model is composed of mechanically ice-like phases, which is considerably more than the upper bound of ~25 vol.% ice estimated by Fu et al. (2017). This result is consistent with the variations in ice content in Sizemore et al. (2018) with more ice observed in association with large craters and basins.

Curiously, of the planetary objects listed in Table 1, Tethys (mean diameter 1,062 km) is closest in size to Ceres (mean diameter 946 km), yet of the icy satellites, its flexural rigidity is the most unlike Ceres. Ganymede, Europa, and Enceladus, whose flexural rigidities are Ceres-like, are all either much larger or much smaller than the dwarf planet. Additionally, these icy moons are all known to have subsurface oceans and believed to have relatively high (tens to hundreds of milliwatts per square meter) modern and/or historical heat fluxes (Bland et al., 2017; Giese et al., 2008; Ruiz, 2005). Tethys likely has no such ocean (Matson et al., 2009).

The similarity of Nar Sulcus to these ocean worlds is most likely due to a combination of its warm thermal environment in the main belt and the peculiar "dirty ice" composition of its surface layer. The average surface temperature on Ceres relative to Enceladus and Tethys is nearly 100 K greater. This dramatically reduces the depth to the ductile layer, which in turn limits the brittle thickness at Nar Sulcus compared to these icy moons for a given heat flux (assuming an ice dominated rheology). Giese et al. (2008) reported heat fluxes in the range 200–270 mW/m^2 for extensionally faulted terrain on Enceladus, so while the elastic properties of Nar Sulcus and Enceladus are very similar, their required formational heat fluxes likely are not. The opposite is true for Tethys, where Giese et al. (2007) reported heat fluxes in the range 18–30 mW/m^2, which are plausibly similar to the historical heat flux at Nar Sulcus, but whose cold, frozen elastic layer is inferred to be between 4.9 and 7.2 km thick. The increased ductility on Ceres is only partially compensated by the increased strength of the cerean near surface due to its silicate component. The potential presence of brines and other salty ice phases near their homologous temperatures within the mechanical layer below Nar Sulcus may further limit the depth to the ductile layer.

Giese et al. (2008) found that including a porosity estimate in their calculations of the heat flux at Harran Sulci, Enceladus, decreased the derived values by a maximum of around one order of magnitude compared to the nonporous cases. However, they cautioned against interpreting their result as being reflective of the true effect of porosity on the thermal conductivity of Enceladus. This reduction in heat flow is due to the insulating effects of increased void space, which in general apply to all solar system objects. If the reduction in thermal conductivity due to porosity on Ceres is proportionally similar to that of what Giese et al. (2008) estimated for Enceladus, then all the parameter combinations in Figure 3 would become geologically plausible in the context of achievable surface heat fluxes on Ceres. The main implications of this would be that the upper layer of Ceres could contain much more silicate-like material than currently expected or that the ancient surface heat flux at Nar Sulcus was no more than a few times the current global average.

6. Conclusions

Through the application of flexural techniques developed for terrestrial settings, we determined that Nar Sulcus is mechanically much more similar to extensional structures on many icy satellites than to their counterparts on the silicate-dominated planets. The characteristics of the faults in Nar Sulcus are consistent with a thin/weak elastic layer approximately 190–590 m thick. The corresponding mechanical layer is 2.9–9.5 km thick. Based on our modeled T_e range, geologic context, and genetic thermal models, we interpret the surface heat flux at Nar Sulcus during its formation to have been ~10–100 mW/m^2. This range is between one and two orders of magnitude larger than the predicted average surface heat flux during the last ~800 Myr, although accurately including the effects of porosity could significantly reduce these values. In combination with the observed variability of the heat flux with changing grain size, this further underscores the importance of knowing both the porosity structure and grain size distribution for thermal modeling of Ceres. This interpreted heat flux range is consistent with a mechanical layer that contains no more than ~30 vol.% mechanically silicate-like phases. If the higher than expected historical heat flux at Nar Sulcus is true, it may plausibly be explained by solid-state diapirism, laccolith formation from cryomagma sourced from either endogenic reservoirs or impact melt, and/or residual heat from the emplacement of Urvara/Yalode Smooth Material from the Urvara-forming impact.

Acknowledgments
We thank NASA, DLR, MPS, and INAF as well as all the Dawn flight, instrument, and science teams. This article benefited from reviews by P. Helfenstein and one anonymous reviewer. All data utilized are available on NASA's PDS Small Bodies Node. This research was funded by the Dawn Mission Science Team, which is supported by NASA's Discovery program.

References

Beeman, M., Durham, W. B., & Kirby, S. H. (1988). Friction of ice. *Journal of Geophysical Research*, *93*(B7), 7625–7633. https://doi.org/10.1029/JB093iB07p07625

Biren, M. B., van Soet, M., Wartho, J. -A., & Spray, J. G. (2014). Dating the cooling of exhumed central uplifts of impact structures by the (U–Th)/He method: A case study at Manicouagan. *Chemical Geology*, *377*, 56–71. https://doi.org/10.1016/j.chemgeo.2014.03.013

Bland, M. T., Singer, K. N., McKinnon, W. B., & Schenk, P. M. (2017). Viscous relaxation of Ganymede's impact craters: Constraints on heat flux. *Icarus*, *296*, 275–288. https://doi.org/10.1016/j.icarus.2017.06.012

Bland, M. T., Sizemore, H. G., Buczkowski, D. L., Sori, M. M., Raymond, C. A., King, S. D., & Russell, C. T. (2018). Why is Ceres lumpy? Surface deformation induced by solid-state subsurface flow. Paper presented at Lunar Planet. Sci. XLIX. Abstract 1627.

Bowling, T. J., Ciesla, F. J., Davison, T. M., Scully, J. E. C., Castillo-Rogez, J. C., Marchi, S., & Johnson, B. C. (2018). Post-impact thermal structure and cooling timescales of Occator crater on asteroid 1 Ceres. *Icarus*. https://doi.org/10.1016/j.icarus.2018.08.028

Buczkowski, D. L., Schmidt, B. E., Williams, D. A., Mest, S. C., Scully, J. E. C., Ermakov, A., et al. (2016). The geomorphology of Ceres. *Science*, *353*(6303). https://doi.org/10.1126/science.aaf4332

Byerlee, J. (1978). Friction of rocks. *Pure and Applied Geophysics*, *116*(4-5), 615–626. https://doi.org/10.1007/BF00876528.

Combe, J. -P., McCord, T. B., Tosi, F., Ammannito, E., Carrozzo, F. G., De Sanctis, M. C., et al. (2016). Detection of local H_2O exposed at the surface of Ceres. *Science*, *353*(6303), aaf3010. https://doi.org/10.1126/science.aaf3010

Combe, J. -P., Raponi, A., Tosi, F., De Sanctis, M. C., Carrozzo, F. G., Zambon, F., et al. (2019). Exposed H_2O-rich areas detected on Ceres with the dawn visible and infrared mapping spectrometer. *Icarus*, *318*, 22–41. https://doi.org/10.1016/j.icarus.2017.12.008

Crown, D. A., Sizemore, H. G., Yingst, R. A., Mest, S. C., Platz, T., Berman, D. C., et al. (2017). Geologic mapping of the Urvara and Yalode Quadrangles of Ceres. *Icarus*. https://doi.org/10.1016/j.icarus.2017.08.004

Durham, W. B., Kirby, S. H., & Stern, L. A. (1992). Effects of dispersed particulates on the rheology of water ice at planetary conditions. *Journal of Geophysical Research*, *97*(E12), 20,883–20,897. https://doi.org/10.1029/92JE02326

Ermakov, A. I., Fu, R. R., Castillo-Rogez, J. C., Raymond, C. A., Park, R. S., Preusker, F., et al. (2017). Constraints on Ceres' internal structure and evolution from its shape and gravity measured by the Dawn spacecraft. *Journal of Geophysical Research: Planets*, *122*, 2267–2293. https://doi.org/10.1002/2017JE005302

Fassett, C. I., & Head, J. W. III (2008). The timing of martian valley network activity: Constrains from buffered crater counting. *Icarus*, *195*(1), 61–89. https://doi.org/10.1016/j.icarus.2007.12.009

Fu, R. R., Ermakov, A. I., Marchi, S., Castillo-Rogez, J. C., Raymond, C. A., Hager, B. H., et al. (2017). The interior structure of Ceres as revealed by surface topography. *Icarus*, *476*, 153–164. https://doi.org/10.1016/j.epsl.2017.07.053

Giese, B., Wagner, R., Hussmann, H., Neukum, G., Perry, J., Helfenstein, P., & Thomas, P. C. (2008). Enceladus: An estimate of heat flux and lithospheric thickness from flexurally supported topography. *Geophysical Research Letters*, *35*, L24204. https://doi.org/10.1029/2008GL036149

Giese, B., Wagner, R., Neukum, G., Helfenstein, P., & Thomas, P. C. (2007). Tethys: Lithospheric thickness and heat flux from flexurally supported topography at Ithaca Chasma. *Geophysical Research Letters*, *34*, L21203. https://doi.org/10.1029/2007GL031467

Goldsby, D. L., & Kohlstedt, D. L. (2001). Superplastic deformation of ice: Experimental observations. *Journal of Geophysical Research*, *106*(B6), 11,017–11,030. https://doi.org/10.1029/2000JB900336

Grott, M., Hauber, E., Werner, S. C., Kronberg, P., & Neukum, G. (2005). High heat flux on ancient Mars: Evidence from rift flank uplift at Coracis Fossae. *Geophysical Research Letters*, *32*, L21201. https://doi.org/10.1029/2005GL023894

Hayne, P. O., & Aharonson, O. (2015). Thermal stability of ice on Ceres with rough topography. *Journal of Geophysical Research: Planets*, *120*, 1567–1584. https://doi.org/10.1002/2015JE004887

Hiesinger, H., Marchi, S., Schmedemann, N., Schenk, P., Pasckert, J. H., Neesemann, A., et al. (2016). Cratering on Ceres: Implications for its crust and evolution. *Science*, *353*(6303), aaf4759. https://doi.org/10.1126/science.aaf4759

Hughson, K. H. G., Russell, C. T., Williams, D. A., Buczkowski, D. L., Mest, S. C., Pasckert, J. H., et al. (2018). The Ac-5 (Fejokoo) quadrangle of Ceres: Geologic map and geomorphological evidence for ground ice mediated surface processes. *Icarus*, *316*, 63–83. https://doi.org/10.1016/j.icarus.2017.09.035

Kneissl, T., Michael, G. G., Platz, T., & Walter, S. G. H. (2015). Age determination of linear surface features using the Buffered Crater Counting approach—Case studies of the Sirenum and Fortuna Fossae graben systems on Mars. *Icarus*, *250*, 384–394. https://doi.org/10.1016/j.icarus.2014.12.008

Kusznir, N. J., Marsden, G., & Egan, S. S. (1991). A flexural-cantilever simple-shear/pure-shear model of continental lithosphere extension: Applications to the Jeanne d'Arc Basin, Grand Banks and Viking graben, North Sea. In A. M. Roberts, G. Yielding, & B. Freeman (Eds.), *The geometry of normal faults*, *Geological Society, Special Publication* (Vol. 56, pp. 41–60). https://doi.org/10.1144/GSL.SP.1991.056.01.04

Lambeck, K. (1983). Structure and evolution of the intracratonic basins of central Australia. *Geophysical Journal of the Royal Astronomical Society*, *74*, 843–886. https://doi.org/10.1111/j.1365-246X.1983.tb01907

Lowry, A. R., & Smith, R. B. (1994). Flexural rigidity of the Basin and Range-Colorado Plateau-Rocky Mountain transition from coherence analysis of gravity and topography. *Journal of Geophysical Research*, *99*(B10), 20,123–20,140. https://doi.org/10.1029/94JB00960

Matson, D. L., Castillo-Rogez, J. C., Schubert, G., Sotin, C., & McKinnon, W. B. (2009). The thermal evolution and internal structure of Saturn's mid-sized icy satellites. In M. K. Dougherty, L. W. Esposito, & S. M. Krimigis (Eds.), *Saturn from Cassini-Huygens* (pp. 577–612). Dordrecht, Netherlands: Springer. https://doi.org/10.1007/978-1-4020-9217-6_18

McCord, T. B., & Sotin, C. (2005). Ceres: Evolution and current state. *Journal of Geophysical Research*, *110*, E05009. https://doi.org/10.1029/2004JE002244

McNutt, M. K. (1984). Lithospheric flexure and thermal anomalies. *Journal of Geophysical Research*, *89*(B13), 11,180–11,194. https://doi.org/10.1029/JB089iB13p11180

Michael, G. G., Kneissl, T., & Neesemann, A. (2016). Planetary surface dating from crater size-frequency distribution measurements: Poisson timing analysis. *Icarus*, *277*, 279–285. https://doi.org/10.1016/j.icarus.2016.05.019

Nadai, A. (1963). *Theory of flow and fracture of solids* (Vol. II, pp. 250–269). New York: McGraw-Hill.

Nimmo, F., & Pappalardo, R. T. (2004). Furrow flexure and ancient heat flux on Ganymede. *Geophysical Research Letters*, *31*, L19701. https://doi.org/10.1029/2004GL020763

Nimmo, F., Pappalardo, R. T., & Giese, B. (2002). Effective elastic thickness and heat flux estimates on Ganymede. *Geophysical Research Letters*, *29*(7), 1158. https://doi.org/10.1029/2001GL013976

Nimmo, F., & Schenk, P. (2006). Normal faulting on Europa: Implications for ice shell properties. *Journal of Structural Geology*, *28*(12), 2194–2203. https://doi.org/10.1016/j.jsg.2005.08.009

O'Rourke, J. G., & Smrekar, S. E. (2018). Signatures of lithospheric flexure and elevated heat flow in stereo topography at coronae on Venus. *Journal of Geophysical Research: Planets*, *123*, 369–389. https://doi.org/10.1002/2017JE005358

Prettyman, T. H., Yamashita, N., Toplis, M. J., McSween, H. Y., Schorghofer, N., Marchi, S., et al. (2017). Extensive water ice within Ceres' aqueously altered regolith: Evidence from nuclear spectroscopy. *Science*, *355*(6320), 55–59. https://doi.org/10.1126/science.aah6765

Ranalli, G. (1995). *Rheology of the Earth* (2nd ed.). London: Chapman and Hall.

Roatsch, T., Kersten, E., Matz, K.–D., Preusker, F., Scholten, F., Elgner, S., et al. (2016a). Dawn FC2 Derived Ceres HAMO DTM SPG V1.0, DAWN-A-FC2–5-CERESHAMODTMSPG-V1.0, NASA Planetary Data System.

Roatsch, T., Kersten, E., Matz, K.–D., Preusker, F., Scholten, F., Elgner, S., et al. (2016b). Dawn FC2 Derived Ceres Mosaics V1.0, DAWN-A-FC2-5-CERESMOSAIC-V1.0, NASA Planetary Data System.

Ruiz, J. (2005). The heat flow of Europa. *Icarus*, *177*(2), 438–446. https://doi.org/10.1016/j.icarus.2005.03.021

Ruiz, J., McGovern, P. J., & Tejero, R. (2006). The early thermal and magnetic state of the cratered highlands of Mars. *Earth and Planetary Science Letters*, *241*(1-2), 2–10. https://doi.org/10.1016/j.epsl.2005.10.016

Russell, C. T., Raymond, C. A., Ammannito, E., Buczkowski, D. L., De Sanctis, M. C., Hiesinger, H., et al. (2016). Dawn arrives at Ceres: Exploration of a small volatile-rich world. *Science*, *353*(6303), 1008–1010. https://doi.org/10.1126/science.aaf4219

Schmidt, B. E., Hughson, K. H. G., Chilton, H. T., Scully, J. E. C., Platz, T., Nsthues, A., et al. (2017). Geomorphological evidence for ground ice on dwarf planet Ceres. *Nature Geoscience*, *10*(5), 338–343. https://doi.org/10.1038/ngeo2936

Sizemore, H. G., Platz, T., Schorghofer, N., Prettyman, T. H., de Sanctis, M. C., Crown, D. A., et al. (2017). Pitted terrains on (1) Ceres and implications for shallow subsurface volatile distribution. *Geophysical Research Letters*, *44*, 6570–6578. https://doi.org/10.1002/2017GL073970

Sizemore, H. G., Schmidt, B. E., Buczkowski, D. A., Sori, M. M., Castillo-Rogez, J. C., Berman, D. C., et al. (2018). A Global Inventory of Ice-Related Morphological Features on Dwarf Planet Ceres: Implications for the evolution and current state of the cryosphere. *Journal of Geophysical Research: Planets*, *123*. https://doi.org/10.1029/2018JE005699

Stein, N. T., Ehlmann, B. L., Palomba, E., De Sanctis, M. C., Nathues, A., Hiesinger, H., et al. (2017). The formation and evolution of bright spots on Ceres. *Icarus*. https://doi.org/10.1016/j.icarus.2017.10.014

Travis, B. J., Bland, P. A., Feldman, W. C., & Sykes, M. V. (2018). Hydrothermal dynamics in a CM-based model of Ceres. *Meteoritics and Planetary Science*, *53*(9), 2008–2032. https://doi.org/10.1111/maps.13138.

Walcott, R. I. (1970). Flexural rigidity, thickness, and viscosity of the lithosphere. *Journal of Geophysical Research*, *75*(20), 3941–3954. https://doi.org/10.1029/JB075i020p03941

Weissel, J. K., & Karner, G. D. (1989). Flexural uplift of rift flanks due to mechanical unloading of the lithosphere during extension. *Journal of Geophysical Research*, *94*(B10), 13,919–13,950. https://doi.org/10.1029/JB094iB10p13919

Yasui, M., Schulson, E. M., & Renshaw, C. E. (2017). Experimental studies on mechanical properties and ductile-to-brittle transition of ice-silica mixtures: Young's modulus, compressive strength, and fracture toughness. *Journal of Geophysical Research: Solid Earth*, *122*, 6014–6030. https://doi.org/10.1002/2017JB014029